A Tilt, Soil Moisture, and Pore Water Pressure Sensor System for Slope Monitoring Applications

Rosanno JC de Dios[1], Jason Enriquez[1], Francis Gabriel Victorino[1], Earl Anthony Mendoza[1], Marc Caesar Talampas[1*], Joel Joseph S. Marciano Jr[2]

[1]Instrumentation, Robotics and Control Laboratory, [2]Wireless Communications Engineering Laboratory
Electrical and Electronics Engineering Institute, University of the Philippines, Diliman Quezon City 1101
*Corresponding author: marct@eee.upd.edu.ph

ABSTRACT

This paper describes the design, implementation and characterization of a sensor network intended for monitoring of slope deformation and potential failures. The sensor network system consists of a tilt and moisture sensor column, a pore water pressure sensor column and a personal computer for data storage and processing. The tilt sensor column consists of several pipe segments containing tri-axial accelerometers and signal processing electronics. Each segment is joined together by flexible joints to allow for the column to deform and subsequently track underground movement. Capacitive-type sensors for soil moisture measurement are also included in the sensor column, which are used to measure the soil moisture at different depths. The measurements at each segment are transferred via a Controller Area Network (CAN) bus, where the CAN master node is located at the top of the column above ground. The CAN master node transmits the collected data from the slave nodes via a wireless connection to a personal computer that performs data storage, processing and display via a Python-based graphical user interface (GUI). The entire system was deployed and characterized on a small-scale slope model. Slope failure was induced via water seepage and the system was demonstrated to ably measure the inclination and soil moisture content throughout the landslide event.

Keywords: sensor networks, slope monitoring, landslide early warning systems, wireless networks

INTRODUCTION

Approximately one-third of the land area of the Philippines consists of steep mountains and slopes making it prone to landslides that result in significant loss of life and property. While the mechanisms underlying landslides are fairly under-stood, actual prediction or forecasting of landslides has been hindered by the lack of field measurements over large temporal and spatial scales. In order for scientists and engineers to make accurate and timely landslide forecasts, critical data must be made available in real time.

In the Philippine setting, slope deformation, excessive rain-fall and water seepage are said to be major factors in slope failures (Naranjo 2007). Thus, there is a need to conduct further study relating slope deformation to soil moisture content and pore water pressure, factors directly affected by rainfall and water seepage. This paper presents the current status of a research project that aims to develop a cost-effective system for measuring the physical parameters that may indicate impending slope failure. A block diagram of the system is shown in Figure 1. A small-scale slope model was constructed inside a box. Sensor columns for measuring tilt, soil moisture and pore water pressure head were

constructed. Data gathered from the sensor columns are transmitted to a computer for storage and visualization. The implementation details for the components of these sensor columns are discussed in Section II of this paper.
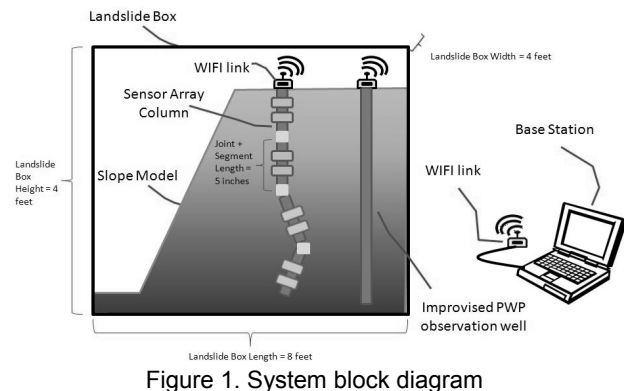

Figure 1. System block diagram

In order to observe slow movements such as slope creep, highly sensitive sensors are necessary. These sensors are typically expensive due to their high sensitivity and precision. Aside from slope creep, there is also a need to observe slide and fall movements which are much faster, with a higher acceleration and elongation. Arnhardt and co-workers (Arnhardt, et. al. 2007) summarized possible landslide movements and the capabilities of different sensors to detect these movements. They concluded that accelerometers are cost-effective means of detecting both creep and slide and fall movements, compared to more expensive displacement transducers and angle sensors. Their work justifies the use of accelerometers for cost-effective soil mass movement detection.

Abdoun et.al. developed the ShapeAccelArray, a micro- electromechanical system (MEMS) accelerometer array that is designed to monitor land displacement and soil acceleration (Abdoun, Danisch & Ha 2005). The array segments were interconnected with flexible joints in order for the instrument to be able to faithfully follow soil movement. The design of the sensor array column is shown in Figure 2. The ShapeAccelArray lacks integrated soil moisture sensors, which can provide additional data that relates slope movement to soil moisture content at different depths.

In slope stability monitoring, it is essential not only to have knowledge on slope deformation or movement but also on soil moisture content. Some

methods such as calculation of precipitation (rainfall density) are normally done to evaluate occurrence of landslides. However, such a method offers little precision since landslides are more directly related to water content of soil rather than rainfall density (Chuang 2003). The accuracy of a landslide warning system can be improved if sensors are installed to measure water content of soil in different depths and locations.
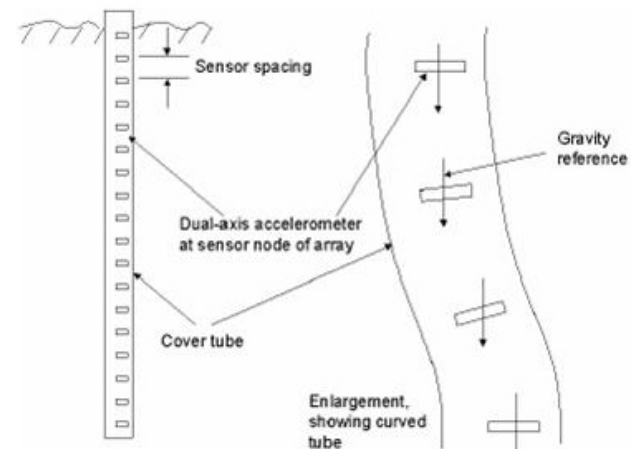

Figure 2. Design of the ShapeAccelArray

Wobschall (1978) describes an approach to minimize measurement sensitivity due to soil type. Both field implantable and laboratory sensors were developed. Measurements were facilitated using a high frequency (31 MHz) Colpitts oscillator. The change in dielectric constant reflects a change in capacitance, which in turn creates a shift in the frequency of the signal generated by the oscillator. The soil's dielectric constant is composed both of a real (dielectric property) and imaginary part (conductivity). Using high frequencies for the oscillator (above 10 MHz) is said to minimize conductivity effects on dielectric measurements (Johnson, Thiel & James 2002). While conductivity can also be an indicator of moisture content, the minimization of its effects is desired because it is a soil type dependent parameter. A frequency at this range is advantageous to use for our system to deal with the soil type sensitivity issue.

The capacitive sensor is coupled to the oscillator circuit via a capacitor T network. This type of coupling is noted to also minimize the effects of soil conductivity on measurements (Wobschall 1978). The sensor is tested extensively in a soils laboratory and in four field locations. Results showed that there

are only small variations in the calibration curves of different soils at low moisture measurements (where conductance is low). However, soils with high conductivity properties such as clay appear to need specific calibration especially at high moisture measurements (where conductance is high). A more recent work of Wobschall together with Lakshmanan (Wobschall & Lakshmanan 2005) also implements the coupling capacitor T network. Figure 3 shows the T-coupling network as part of their system. Switches were used at the sensor side to fix the problem of frequency drift with time. A standard value capacitor is alternately switched in order to normalize measured values.
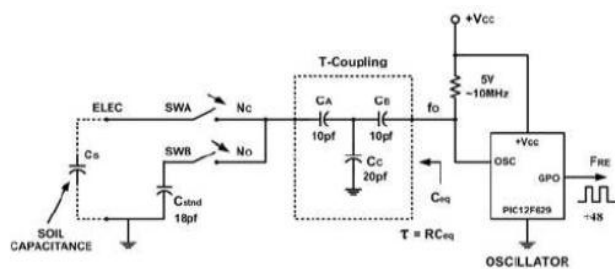

Figure 3. Capacitor T-coupling network

Instead of using LC oscillators, their system made use of the microcontroller's RC oscillator for simplicity. A PIC microcontroller which has oscillators capable of working at high enough frequencies (above 10 MHz) was used. A PIC microcontroller is also used in our system, taking care of both tilt and soil moisture content measurements at various depths underground. An added feature is seen in their system, allowing for wireless data collection via radio communication over a range of 30 to 100 meters. Our system also allows data collection in the same manner except that it uses a WiFi module to transmit data to a base station.

The conditions under which their system has been tested are not explicitly stated. Their results showed that their sensor could take measurements over a wide range of 0 to 45% (water in soil by volume) with good reproducibility. It has been further stated that soil specific calibration is still needed to achieve such good results.

METHODOLOGY

The box in which the slope model was constructed has dimensions of 2.43 m x 1.21 m x 1.21 m. The design and dimensions of the box are similar to that used by Orense et. al. (2004). Considering the small size of the box, the sensor columns had to be made as small as possible to minimize the mitigating effect it might have on the landslides to be induced on the slope model. The columns were made out of PVC segments with an inner diameter of 19 mm. Each segment of the sensor column contains a microcontroller, an accelerometer, a soil moisture sensor, and a CAN transceiver. Surface mount packages were selected for most of the electronic components to minimize the board size, allowing the board to snugly fit inside the PVC segments. An image of the circuit board is shown in Figure 4.
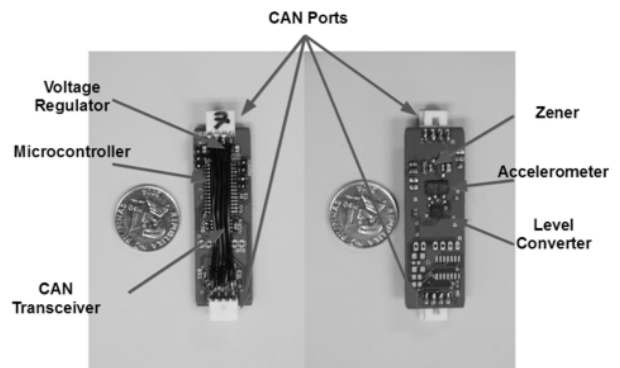

Figure 4. Circuit board for tilt and soil moisture sensor

Soil Moisture Sensor

Figure 5 shows the block diagram of the soil moisture sensor design. A capacitive sensor was used and connected to an oscillator circuit. The frequency of the output signal is then measured using a microcontroller. The frequency shift, which results from the connection of the sensor to the oscillator, is taken as a measure of the soil moisture content.
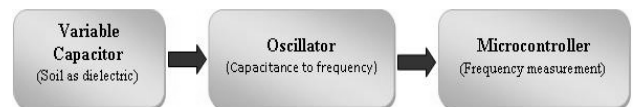

Figure 5. Soil moisture sensor design

The physical design with the corresponding dimensions of the soil moisture sensor is shown in Figure 6. The capacitance sensor is located at the middle section of a 10.16 cm PVC pipe segment. Inexpensive materials such as aluminum duct tape, flat antenna wires for a predictable stray

capacitance, and acrylic epoxy paint for insulation, were used to build the sensor. Eight sensors were constructed and initially tested using their measured capacitances in air and wet soil. Figure 7 shows the results obtained from the constructed sensors. The average values for the capacitances of the sensors in air and wet soil are 2.7 pF and 333.8 pF, respectively. As expected, the capacitance values of the sensors are directly proportional to the soil moisture content. It can also be seen that the capacitance values of the constructed sensors are relatively close to each other.
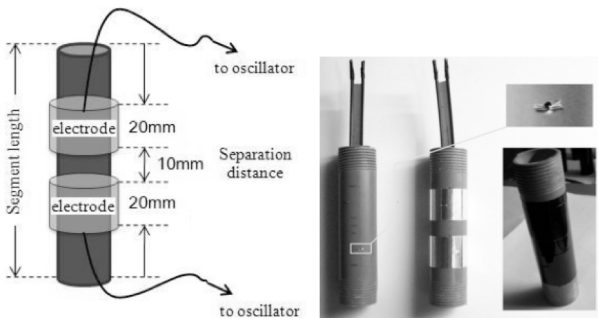

Figure 6. Soil moisture sensor dimensions and photo

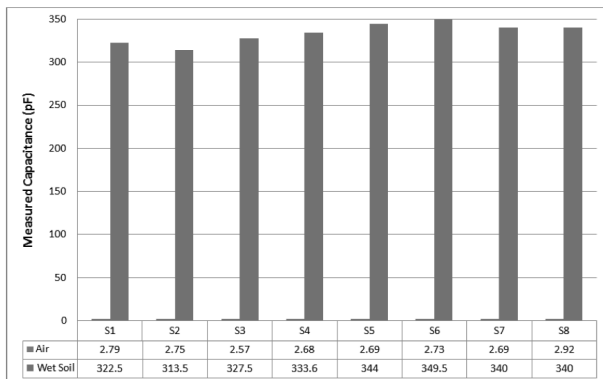|	S1	S2	S3	S4	S5	S6	S7	S8
Air	2.79	2.75	2.57	2.68	2.69	2.73	2.69	2.92
Wet Soil	322.5	313.5	327.5	333.6	344	349.5	340	340

Figure 7. Capacitance ranges of sensors

The sensors were used as part of an RC oscillator using CMOS inverter gates. As recommended by (Wobschall 1978), a T-coupling network was used to minimize the conductivity effects encountered when taking soil moisture measurements.

Figure 8 shows how a frequency shift measurement is made. Multiple measurements are averaged to minimize possible measurement errors. The number 30 was experimentally determined as sufficient, although a more optimal number may be used in the future. The microcontroller first takes the average of 30 measurements of the oscillator frequency with the sensor disconnected from the rest of the circuit. After taking the measurements, the microcontroller then activates a switch, which connects the sensor to the oscillator. The average of 30 measurements is again taken. The difference between the frequency measurements is then sent to a computer, which then computes the corresponding soil moisture measurement.
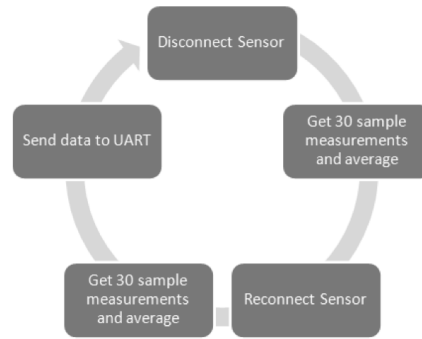

Figure 8. Frequency Measurement Cycle

The performance of the sensor was characterized using three soil types, namely Ottawa sand, silty clay (Diliman campus soil) and Kaolinite clay. Three prototype sensors were tested to evaluate measurement reproducibility. The measurements are taken at 20% saturation intervals for each soil type. The degree of soil compaction affects the measured frequency shifts of the sensor. To mitigate this effect, every test was done using a constant *in situ dry density*. Dry density is the density of soil at zero saturation level (driest condition). Figure 9 shows the characterization setup.
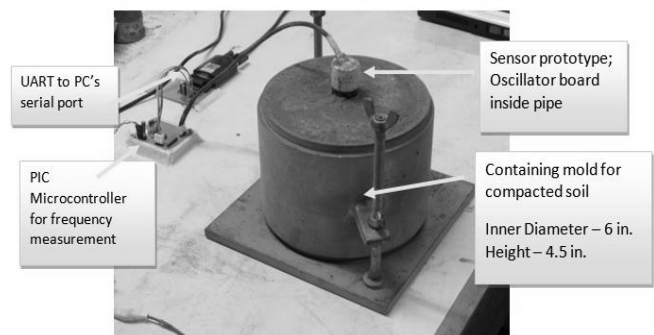

Figure 9. Soil moisture sensor characterization setup

While care was taken to maintain the same degree of soil compaction during the tests, errors due to variances in compaction were encountered, affecting the reproducibility of the measurements. The degree of compaction is a function of soil density, which varies for different soil types. Thus, soil type-

specific calibration is still required for the sensor. Table 1 shows the minimum, maximum, and average frequency shifts measured by the three prototype sensors for varying levels of saturation for the different soil types. This data is plotted in Figure 10, showing different characterization curves for each soil type. It can be seen from Figure 10 that the frequency shift measurements for different soil types are, for most points, significantly different from each other. There is a slight overlap of error bars at saturation levels of 0%, 80%, and 100%. From the characterization curves, piecewise functions can be obtained relating the frequency shifts to % saturation levels.

Table 1. Characterization results for different soil types

| Satur ation (%)	Frequency Shift (MHz)								
	Ottawa Sand			Diliman Soil			Kaolinite Clay		
	Min	Max	Ave.	Min	Max	Ave.	Min	Max	Ave.
0	2.008	2.112	2.076	4.834	5.197	4.979	2.620	2.670	2.642
20	2.731	2.816	2.773	8.541	8.800	8.631	5.430	6.220	5.918
40	3.719	3.876	3.813	8.742	9.014	8.847	7.240	7.810	7.618
60	5.668	6.022	5.856	8.632	8.767	8.701	8.168	8.320	8.230
80	5.787	6.135	5.964	8.906	9.046	8.995	8.573	9.010	8.788
100	5.672	5.948	5.824	8.993	9.168	9.103	8.910	9.010	8.997
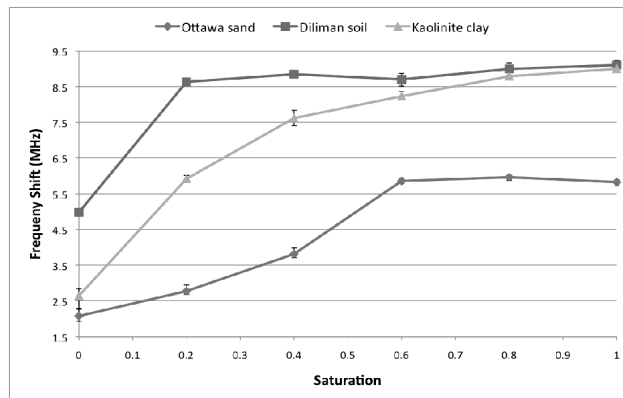
Figure 10. Average characterization curves for different soil types

It was observed that the sensor becomes less sensitive at higher saturation levels. This trend is clearly seen in Figure 10, in which the slopes of the characterization curves are less steep as saturation levels are increased. It was also observed that higher measurements are acquired when the degree of compaction is higher, effectively shifting the entire curve upwards.

The results of Figure 10 in piecewise equation form as follows:

$$\% Saturation_{sand} = \begin{cases} 0 & f_{shift} \leq 2.076MHz \\ 31.33f_{shift} - 65.05 & 2.076 < f_{shift} \leq 2.773MHz \\ 21f_{shift} - 36.4 & 2.773 < f_{shift} \leq 3.813MHz \\ 11.09f_{shift} + 1.38 & 3.813 < f_{shift} \leq 5.782MHz \\ 47.92f_{shift} - 211.6 & 5.782 < f_{shift} \leq 6.238MHz \\ 15.87f_{shift} - 11.65 & 6.238 < f_{shift} \leq 7.035MHz \\ 100 & f_{shift} > 7.035MHz \end{cases} \quad (1)$$

$$\% Saturation_{Diliman} = \begin{cases} 0 & f_{shift} \leq 4.979MHz \\ 5.48f_{shift} - 27.26 & 4.979 < f_{shift} \leq 8.631MHz \\ 92.45f_{shift} - 777.9 & 8.631 < f_{shift} \leq 8.847MHz \\ 271.5f_{shift} - 2362 & 8.847 < f_{shift} \leq 8.995MHz \\ 184.6f_{shift} - 1581 & 8.995 < f_{shift} \leq 9.103MHz \\ 100 & f_{shift} > 9.103MHz \end{cases} \quad (2)$$

$$\% Saturation_{clay} = \begin{cases} 0 & f_{shift} \leq 2.642MHz \\ 6.105f_{shift} - 16.13 & 2.642 < f_{shift} \leq 5.918MHz \\ 11.76f_{shift} - 49.59 & 5.918 < f_{shift} \leq 7.618MHz \\ 32.7f_{shift} - 209.1 & 7.618 < f_{shift} \leq 8.230MHz \\ 35.82f_{shift} - 234.8 & 8.230 < f_{shift} \leq 8.788MHz \\ 96f_{shift} - 763.7 & 8.788 < f_{shift} \leq 8.997MHz \\ 100 & f_{shift} > 8.997MHz \end{cases} \quad (3)$$

The resolution of the sensor is determined by the smallest frequency shift that the microcontroller was programmed to resolve, which is 1 KHz. By observing the smallest frequency change in the characterization curves presented in Figure 10, we can determine the sensor resolution in terms of % saturation. In determining the smallest frequency change from Figure 10, we disregard the points at which the frequency shift readings have already settled. For Diliman soil, this occurs at a saturation level of greater than 40%. The average frequency shift change from 20% to 40% saturation levels for Diliman soil is 216 KHz. Solving for the frequency shift per 1% saturation change:

$$\frac{Frequency\ shift}{Saturation\ change} = \frac{216\,KHz}{(40\% - 20\%)} = 10.8\,KHz/1\%\ saturation \quad (4)$$

Since the microcontroller can resolve 1Khz frequency shifts, the resolution can be solved as:

$$Resolution = \frac{1KHz}{10.8KHz/1\%saturation} = 0.092\% \gg 0.1\% \quad (5)$$

The range of the sensor was found to be 0 to 100% saturation, except for Ottawa sand, which leveled off at around 60% saturation. The response time of the sensor was measured at 0.87 seconds.

Tilt Sensor

To detect soil movement, the tilt of each segment of the sensor column was measured using an ST Microelectronics LIS3LV02DL accelerometer. The LIS3LV02DL is a low-voltage digital output tri-axial accelerometer that was configured to measure acceleration within the range of +/-2 g at a sensitivity of 1024 lsb/g. The accelerometer also features internal signal conditioning circuits and a 4-wire SPI digital interface. By using an accelerometer with internal signal conditioning and digital interface, the probability of noise corrupting the acceleration readings is minimized.

The tilt of each segment of the sensor column is determined by measuring the static acceleration due to gravity sensed by the accelerometer. The angle between the longitudinal axis of the segment and the gravity vector is computed as:

$$\theta = \sin^{-1}\left(\frac{accelerometer\ data}{gravity}\right) \times \left(\frac{180}{\pi}\right) \qquad (6)$$

The computation shown is for a single-axis only. To determine the tilt of the segment with respect to another axis of the accelerometer, the same formula is used.
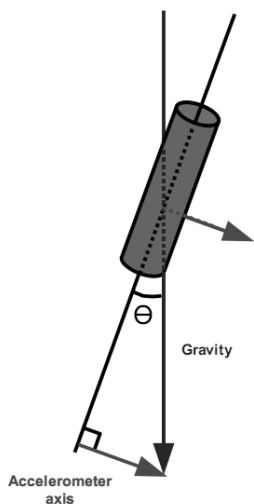

Figure 11. Tilt calculation based on accelerometer data

The tilt sensor was characterized by comparing the measured tilt with the sensor's actual tilt. The results of the characterization are shown in Figure 12. A maximum absolute error of 2° was recorded during characterization.

Pore water pressure sensor

A method for measuring pore water pressure is performed by determining the level of water in an observation well. An observation well was constructed using a 19-mm diameter PVC pipe with a length of 0.61 m. The inside surface of the pipe was lined with two aluminum tape strips as electrodes. A geotextile material was attached to the bottom of the pipe in order to filter out soil particles, ensuring that only water goes up the pipe. Figure 13 shows the constructed pore water pressure sensor.
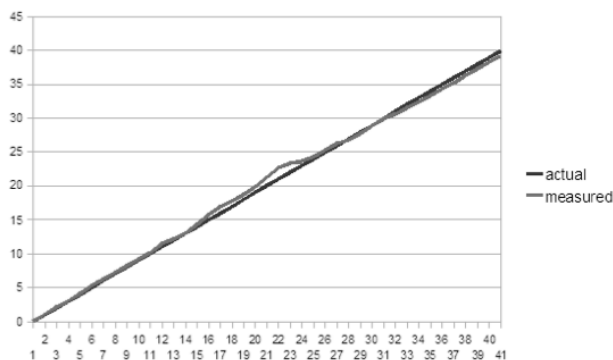

Figure 12. Measured angle vs. actual angle

Figure 13. Pore water pressure sensor

The water level inside the pipe was measured by treating the pipe as a capacitor with air and water as its dielectric materials. A change in the water level inside the pipe produces a change in the pipe's capacitance, which was determined by measuring the electric discharge time of the capacitor. The waveform of the voltage across the capacitor as a measurement is being made is shown in Figure 14. The relationship between the discharge time and the water level was determined by measuring the discharge time for the cases when there is no water inside the pipe and when the pipe has a water level of 60.96 cm. The difference between discharge times were then divided by 60.96 cm to obtain the discharge time change per 1cm change in water level. Figure 15 shows the results of the level sensor accuracy test. For the three trials shown, an average absolute error of 0.89 cm was recorded.
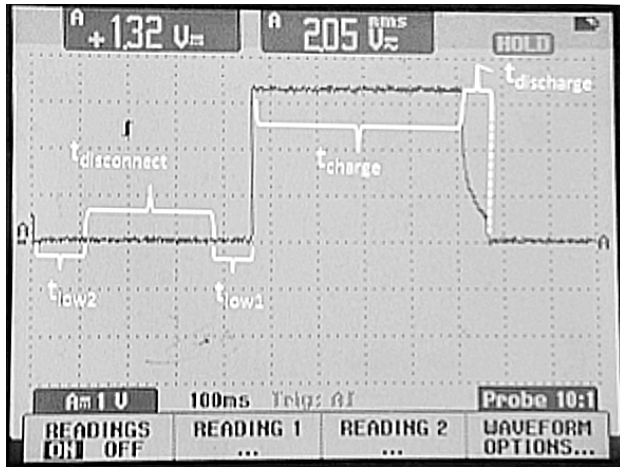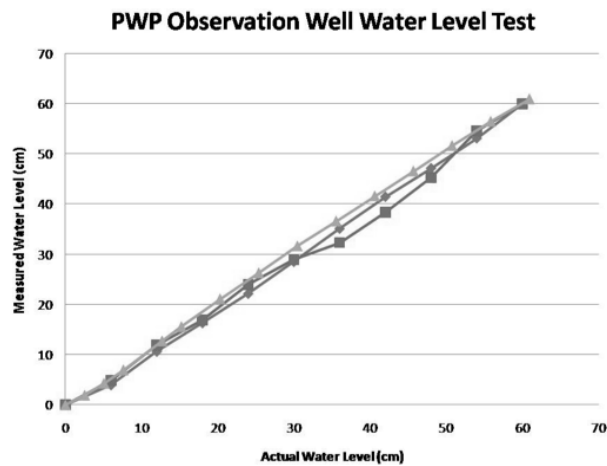
Figure 14. Discharge time measurement cycle

Figure 15. Water level sensor accuracy test

column were connected to a Lantronix WiFi module for wireless connectivity.

Figure 16. CAN bus setup

Sensor Network Communications

Each segment of the sensor column is equipped with a microcontroller that takes sensor readings and enables communication between column segments. Data and control messages are exchanged between different microcontrollers through the Controller Area Network (CAN). The Microchip PIC18F2585 microcontroller was used since it has an internal CAN controller. An MCP2551 CAN transceiver was used to interface the microcontroller to the differential CAN bus. Figure 16 shows how the segment microcontrollers are connected to the 4-wire CAN bus. The CAN bus was configured to operate at a nominal bit rate of 40 Kb/s. This bitrate is sufficient for the application since the sensors of each segment are only sampled at 1 Hz.

The master microcontrollers of the soil moisture and tilt sensor column and pore water observation well

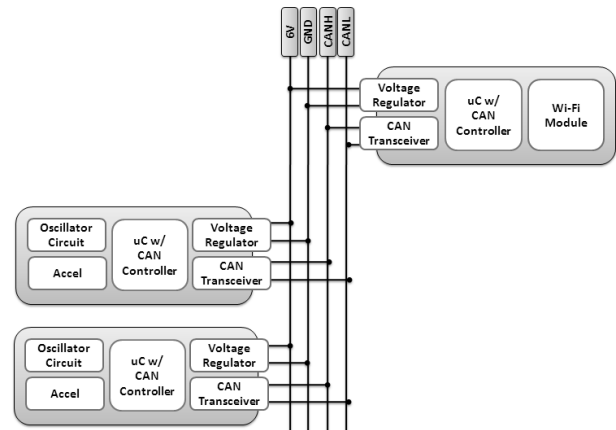## Sensor Column Packaging

The circuit board for the sensors and microcontroller is fitted into a PVC pipe segment 10.16 cm in length and with an inner diameter of 19 mm. Care was taken to ensure that the circuit boards are aligned along the same axis while constructing the column. The orientations of the segments being joined are adjusted until the tilt readings from their accelerometers are the same. This ensures that the segments are aligned along the X, Y, and Z-axis.

Heat-shrinkable rubber tubing was used to form the joints of the sensor column. This allowed the column to easily bend upon movement of the model slope. An extra layer of rubber tubing was used to sheath the entire column for additional strength and waterproofing. This is needed so that the sensor column can be used in multiple experiments before the packaging breaks down. In a real-world deployment, the sensor column will no longer be removed for reuse once it is installed. Figure 17 shows the prototype sensor column and its dimensions.

Graphical User Interface

A graphical user interface (GUI) was developed as a tool to help visualize the data gathered from the sensor columns. A screenshot of the custom graphical user interface is seen in Figure 18. The GUI plots the cumulative displacement of the sensor column along the XZ and YZ planes, as well as soil

moisture and pore water pressure head data. Users of the GUI can choose from three operation modes: real-time single plotting, real-time cumulative displacement plotting, and database plotting. Real-time single plotting allows the user to view the data as soon as the sensor column sends them. Real-time plots are updated at a rate of 1 Hz. Real-time cumulative displacement plotting is similar to real-time single plotting, but also displays the five most recent displacement plots. This allows users to see the progression of the slope movement from the past five readings. Database plotting allows the user to specify the time period from which to generate the plots.
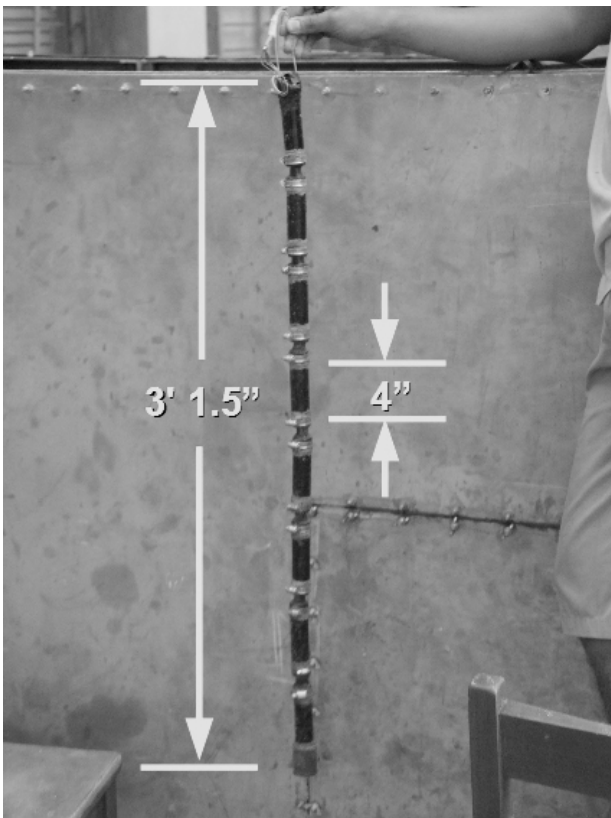

Figure 17. Tilt and soil moisture sensor column dimensions

SMALL-SCALE SLOPE MODEL TEST

For the small-scale slope model test, the sensor columns were first installed inside a box. The pore water pressure column was placed at the leftmost side of the box, where the berm of the small-scale slope model was to be constructed. The tilt and soil moisture sensor column was placed around ¼ of the way between the berm and the toe of the small-scale slope model. Once the columns were firmly secured,

the slope model was built using Porac sand. Porac sand is readily available as it is derived from lahar from the Pinatubo volcano. The tilt and soil moisture sensor column contained seven sensor nodes, S1 to S7, with S1 at the top and S7 at the bottom.

To simulate the water seepage conditions that occur prior to a landslide, two chambers were integrated at the sides of the box. These two chambers are separated from the main chamber containing the sand by a porous geotextile material. During the course of the experiment, water will be allowed to seep from the left chamber into the main chamber, and out from the main chamber to the right chamber.

A video camera was placed two meters away from the box to visually document the water seepage and soil movement. The images captured by the camera were used to correlate and compare the visual data with the data gathered by the sensor columns. Figure 19 shows the setup of the landslide box.

The test was started with the sensors sampling at a rate of 1 Hz while the water level inside the left chamber was increased at a constant rate. Water was allowed to seep across the slope until it has saturated the slope's toe. Once the toe was saturated, the water level was decreased to prevent the slope from rapid failure. An immediate landslide event was undesirable for this initial experiment as the primary objective was to exercise and test the sensors. The effect of decreasing the water level was to impress different soil moisture levels upon different parts of the slope, allowing the sensors to register different soil moisture readings at different depths. After exercising the soil moisture sensors, the water level was increased again until a landslide occurred. Table 2 shows the summary of events for the initial experiment.

Figure 20 shows the raw soil moisture sensor data acquired for approximately 2.5 hrs. The frequency shifts recorded by the seven soil moisture sensors can be converted into saturation level readings by plugging them into the piecewise equations shown in (1). By following the sequence of events listed in Table 1, the sensors were verified to work as each segment detected a rise in soil moisture as the water rose inside the tank. The visual data from the landslide box (water height) agrees with the plot
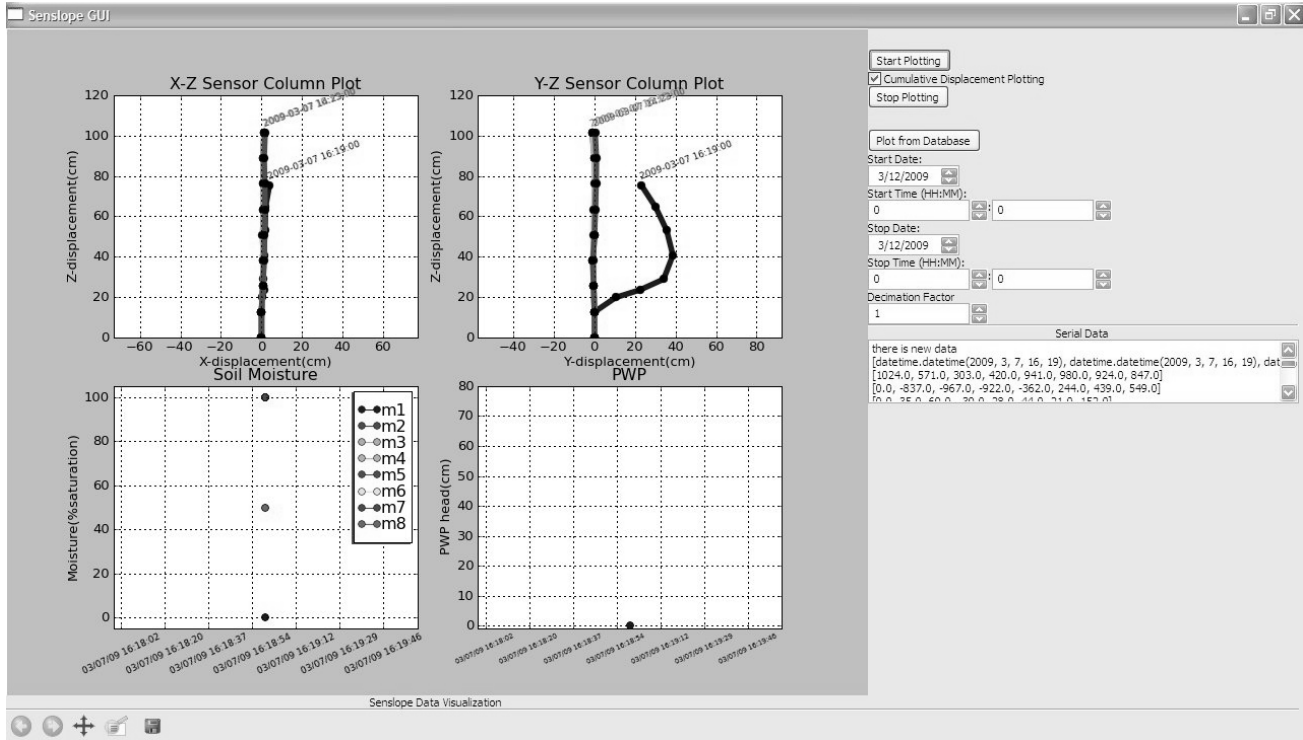
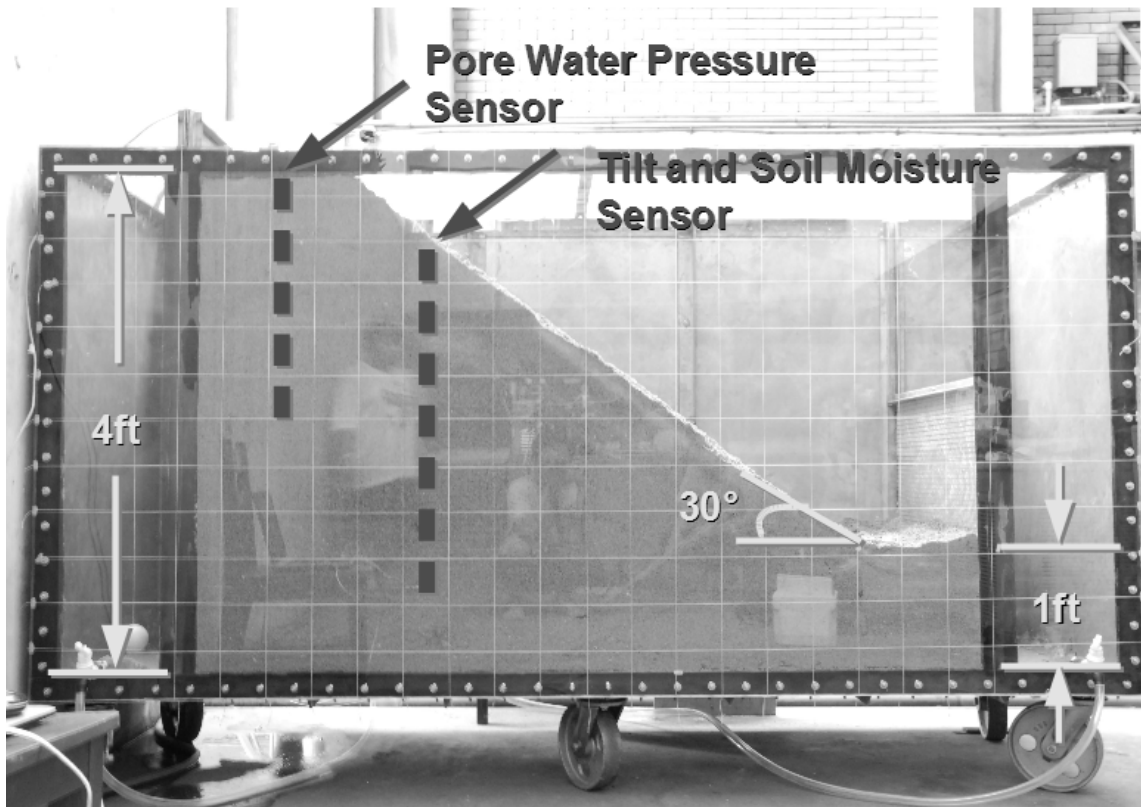Figure 18. Graphical User Interface (GUI) screenshot.

Figure 19. Small-scale model setup.

presented in Figure 20. Right before the landslide event occurred, it was noted that there was a sharp increase in the measured saturation level at the location of sensor S3.

Table 2. Events and milestones for the landslide experiment.

Time	Water Level	Notes
14:22:31	0 m	Start of experiment. Water level starts to increase
14:40:34	0.1 m	Water seepage reaches 0.2 m in height, 0.7 m in length.
15:33:13	0.75 m	Saturation of the slope's toe. Water reaches the other end of the box. Start of water level decrease.
15:41:45	0.5 m	Water at the other end reaches 0.1 m.
15:59:10	0.2 m	Water level increases again.
16:19:04	0.81 m	Start of landslide event.
16:19:09	0.81 m	End of landslide event.

The pore water pressure sensor was buried at the top of the slope up to a depth of 0.61 m. This allowed it to measure the pore water pressure at this depth. A graph of the measurements taken during the small-scale slope model test is shown in Figure 21. From

the measurements made, it can be seen that the expected sensor behavior had been met. As the water level rose beyond 0.61 m, the pore water pressure at that depth also increased. It is interesting to note that before the landslide event, there was a steady rise of pore water pressure. This agrees with the concept that as pore water pressure increases, the pressure pushes away soil particles making soil attraction weaker, and slope failure more probable. As soon as the landslide event occurred, the pressure was released, explaining the sudden dip in the readings of the sensor.

The major landslide movement occurred within the duration of four seconds. Tilt sensor data taken from this duration was used to visualize the movement of the sensor column while the landslide was occurring. Figure 22 shows the deformation experienced by the column during the landslide event. The angles (in degrees) with respect to the vertical are shown for each segment. Comparing the reconstructed column shape from the tilt data with the actual appearance of the sensor column in Figure 23, it can be seen that the tilt sensor data and actual
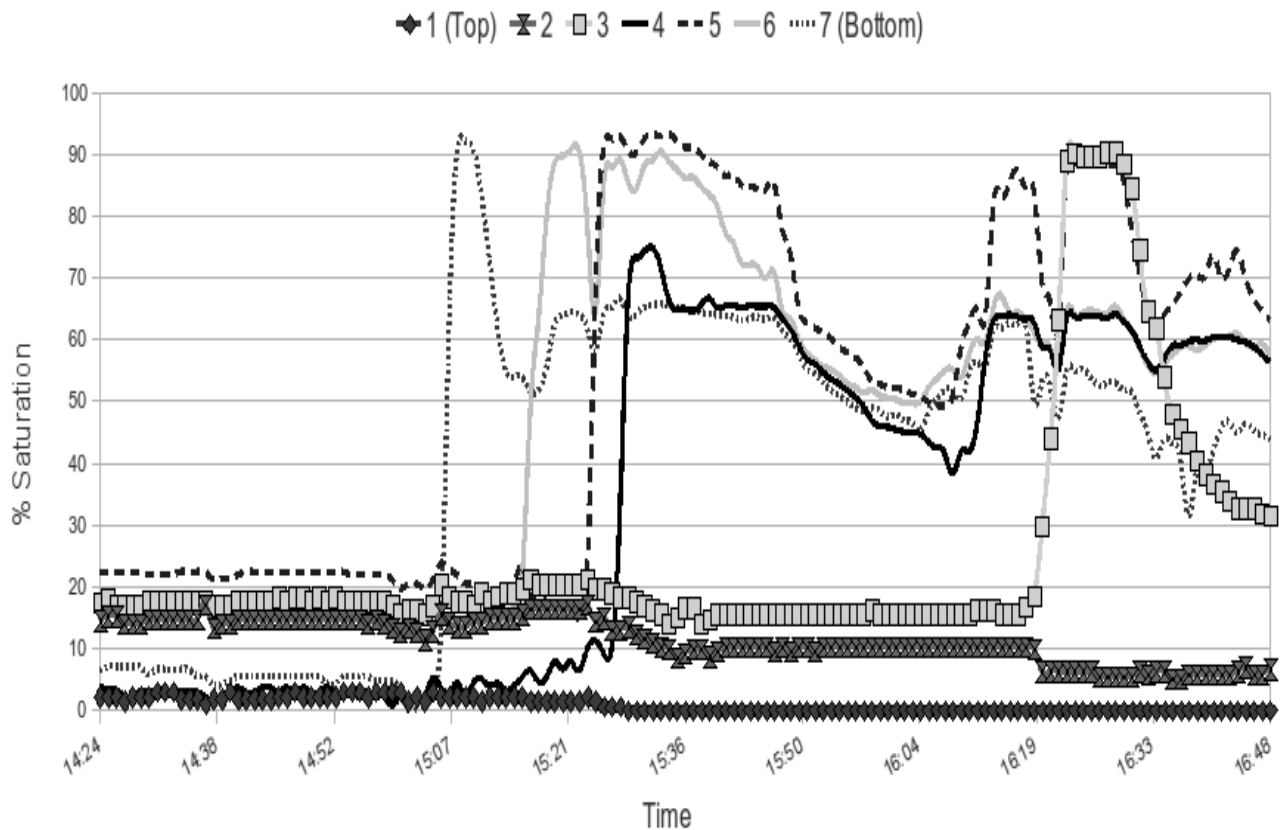

Figure 20. Landslide box soil moisture sensor deployment data.

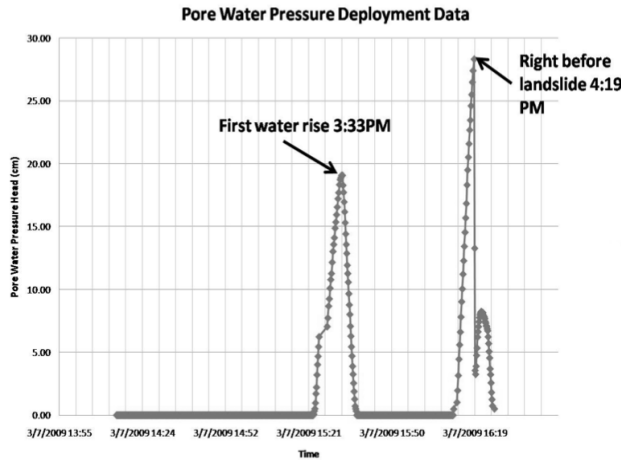tilt of the column are in agreement.

Figure 21. Pore water pressure head.

The slip surface of a landslide is a plane on the slope that separates the sliding part of the slope from the static part. The location of the slip surface of the slope can be estimated from the displacement of the sensor column by noting which segment experienced the maximum displacement from its original position. An estimate of the slip surface location for this initial experiment is shown in Figure 24. Estimation of the slip surface location can be improved by deploying a larger number of tilt sensors underground.
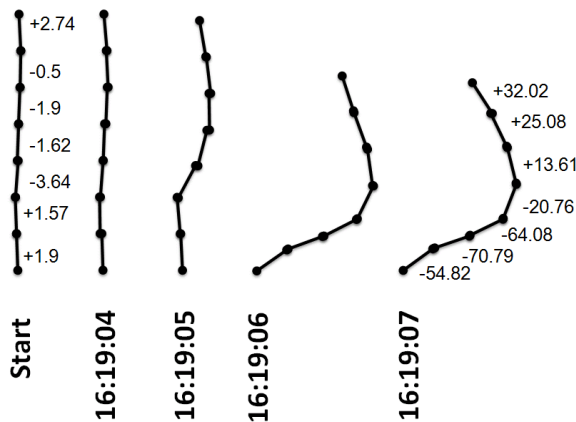

Figure 22. Sensor column movement during induced landslide.

A limitation of typical MEMS accelerometers is that it cannot distinguish between static acceleration (i.e. gravity) and dynamic acceleration. Since static acceleration is used to determine the tilt of each segment of the sensor column, any acceleration not due to gravity will also be represented as a tilt. Thus, the tilt sensor as presently implemented will only yield valid readings when a landslide is sufficiently slow moving.

Tilt sensor data   **Visual data**

Figure 23: Tilt sensor data vs. visual data.

CONCLUSIONS

A sensor network for measuring slope tilt, soil moisture and pore water pressure was designed, developed and tested on a small-scale slope model in a box. An experiment was performed to demonstrate the functionality and capabilities of the sensor network.

The soil moisture sensor can resolve 1% saturation levels within the range of 0-100% at a response time of 0.87 seconds.

The degree of compaction of a given soil sample was found to affect the sensor readings. Since the degree of compaction is a function of the soil density, different soil types will yield different sensor characterization curves. Three different soil types were tested, resulting in different characterization curves due to the varying range of compaction. Measurement reproducibility was also affected by the degree of compaction, higher degrees of compaction resulted in higher soil moisture sensor readings for the same soil type. The sensitivity of the soil moisture sensor was also found to decrease as the saturation level for all soil types were increased.
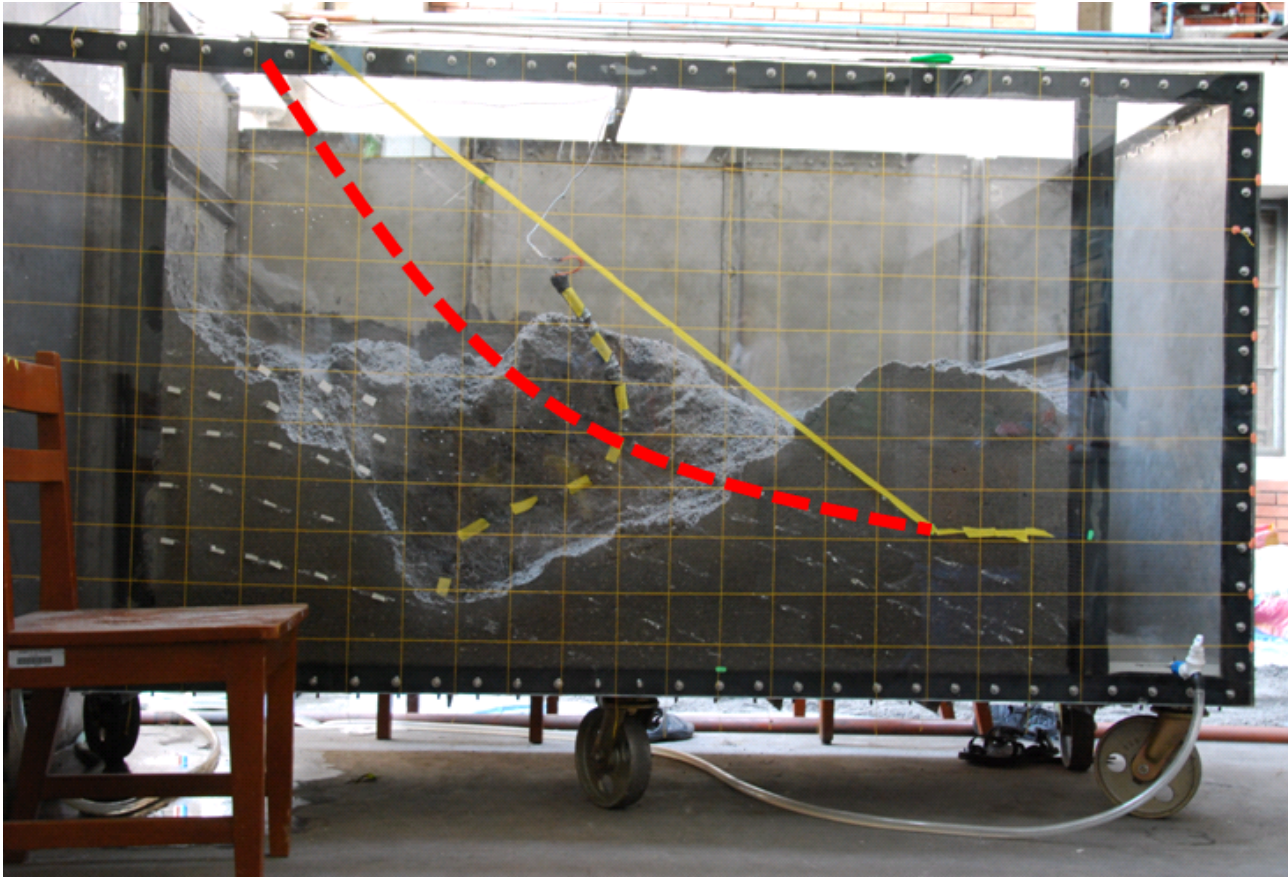
Figure 24. Slip surface location estimate.

It was shown that an electronic pore water pressure observation well could be easily constructed from low cost materials. The pore water pressure sensor was found to have a maximum error of 0.89 cm. During the small-scale slope model test, the sensor was able to measure the sharp increase in pore water pressure right before the occurrence of a landslide event.

Tilt sensors were developed using MEMS accelerometers placed inside each segment of the sensor column. The static acceleration due to gravity was used to determine the tilt angles of each segment with respect to the vertical. An initial experiment performed on a small-scale slope model showed that the tilt sensors can accurately reconstruct the deformation of the column. Inspection of the data recorded by the sensors and the actual deformation of the sensor column showed an agreement between the two. The slip surface location of the landslide can be estimated by noting which segment experienced the maximum displacement from its original position.

A graphical user interface (GUI) was developed as a tool to help visualize the data gathered from the sensor columns. The GUI plots the cumulative displacement of the sensor column along the XZ and YZ planes, as well as soil moisture and pore water pressure head data. Different operating modes allow the user to view data historically or in real-time.

The entire system was tested on a small-scale slope model inside a box. A slope failure was induced by allowing water to seep into the slope. Slope deformations and increases in soil moisture and pore water pressure were detected prior to the landslide event.

FUTURE WORK AND RECOMMENDATIONS

The sensor network is to be installed on a slope at the University of the Philippines Visayas (UPV) Campus, Iloilo, Philippines on January 2010. The

pilot deployment site was selected as it already has a history of slope movement. Two sensor columns will be installed at the slope in the UPV Campus, one at the berm and one at the toe. Each sensor column will be 10 m long. The berm sensor column will have sensor nodes installed every 1m, while the sensor column at the toe will have sensor nodes installed every 0.5 m. Sensor nodes are more closely spaced together at the toe since it was observed during the small-scale experiments that slope movements occur when areas in the toe are nearly saturated. The packaging of the sensor columns will be strengthened further for it to withstand underground deployment. Polyethylene pipes will be used instead of PVC pipes, as these are more flexible and robust.

Refinements in the sensor node firmware are currently underway. Field programmability is a feature that will allow users to modify the firmware of the sensor network through the CAN bus. The addition of this feature will allow users to modify the firmware of the sensor network without having to dismantle its packaging to retrieve the sensor nodes. This is especially useful when firmware updates need to be made on a system already deployed in the field.

To ensure that the sensor network will operate for a long time, alternative power sources such as solar and wind will be tapped. This is necessary to lengthen the sensor network lifetime, allowing it to gather data from slopes that may be experiencing slow moving landslides.

Additional experiments on the small-scale slope model are currently underway.

ACKNOWLEDGEMENT

REFERENCES

L. Naranjo, Connecting Rainfall and Landslides, *NASA Earth Science Data and Services*, September 4, 2007. [Online] Available: http://nasadaacs.eos.nasa.gov/articles/2007/2007_landslides.html [Accessed November 22, 2008].

Arnhardt C., Asch, K., Azzam, R., Bill, R., Fernandez-Stegger, T.M., Hornfeld, S., Kallash, A., Niemeyer, F., Ritter, H., Toloczyki, M., Walter, K. Sensor-Based Landslide Early Warning System - SLEWS, Geotechnologien Science Report, *Early Warning Systems in Earth Management*. pp.75-78, October 2007.

Abdoun, T., Danisch, L., Ha D., Advanced Sensing for Real-Time Monitoring of Geotechnical Systems, *Proceedings of Sessions of the Geo-Frontiers Congress*, 2005.

Chuang, H., United States Patent for an Apparatus for Detecting Saturation of Water in Soil, Patent No.: US 6601440 B1., August 2003.

Wobschall, D., A Frequency Shift Dielectric Soil Moisture Sensor, *IEEE Transactions on Geoscience Electronics*. GE-16(2): 112-118, April 1978.

Johnson, P., Thiel, D., James, D., Contributions to the Measured Capacitance by the Dielectric Properties of Water in Insulated Electrode Soil Moisture Sensors, *Proceedings of IEEE Sensors*, 2002, pp.495-498.

Wobschall, D., Lakshmanan, D., Wireless Soil Moisture Sensor Based on Fringing Capacitance, *Proceedings of IEEE Sensors*, 2005, pp.4.

Orense, R.P., Shimoma, S., Maeda, K. & Towhata. I. 2004. Instrumented model slope failure due to water seepage. *Journal of Natural Disaster Science* 26: 15-26